20. The crystal structure of an Fe(IV)(O)(porphyrin) complex with an Fe–O bond length of 1.604 Å was briefly mentioned in a footnote of Schappacher *et al.* (*39*), but this result has not been subsequently presented in greater detail.
21. S. L. Edwards, N. H. Xuong, R. C. Hamlin, J. Kraut, *Biochemistry* **26**, 1503 (1987).
22. V. Fülöp *et al.*, *Structure* **2**, 210 (1994).
23. C. E. MacBeth *et al.*, *Science* **289**, 938 (2000).
24. M. Costas *et al.*, *J. Am. Chem. Soc.* **123**, 12931 (2001).
25. M. L. Hopper, E. O. Schlemper, R. K. Murmann, *Acta Crystallogr. B* **38**, 2237 (1982).
26. H.-F. Hsu, Y. Dong, L. Shu, V. G. Young Jr., L. Que Jr., *J. Am. Chem. Soc.* **121**, 5230 (1999).
27. F. Ogliaro *et al.*, *J. Am. Chem. Soc.* **122**, 8977 (2000).
28. M. Hata, Y. Hirano, T. Hoshino, M. Tsuda, *J. Am. Chem. Soc.* **123**, 6410 (2001).
29. P. E. M. Siegbahn, *J. Biol. Inorg. Chem.* **6**, 27 (2001).
30. H. Basch, K. Mogi, D. G. Musaev, K. Morokuma, *J. Am. Chem. Soc.* **121**, 7249 (1999).
31. T. Kitagawa, Y. Mizutani, *Coord. Chem. Rev.* **135/136**, 685 (1994).
32. W. Nam, R. Y. N. Ho, J. S. Valentine, *J. Am. Chem. Soc.* **113**, 7052 (1991).
33. S. J. Lange, H. Miyake, L. Que Jr., *J. Am. Chem. Soc.* **121**, 6330 (1999).
34. H. Miyake, K. Chen, S. J. Lange, L. Que Jr., *Inorg. Chem.* **40**, 3534 (2001).
35. K. L. Kostka *et al.*, *J. Am. Chem. Soc.* **115**, 6746 (1993).
36. H. Zheng, S. J. Yoo, E. Münck, L. Que Jr., *J. Am. Chem. Soc.* **122**, 3789 (2000).
37. D. Lee *et al.*, *J. Am. Chem. Soc.* **124**, 3993 (2002).
38. C.-M. Che, K.-Y. Wong, T. C. W. Mak, *J. Chem. Soc. Chem. Commun.* **1985**, 546 (1985).
39. M. Schappacher, R. Weiss, R. Montiel-Montoya, A. Trautwein, A. Tabard, *J. Am. Chem. Soc.* **107**, 3736 (1985).
40. W. T. Oosterhuis, G. Lang, *J. Chem. Phys.* **58**, 4757 (1973).
41. Copies of the data can be obtained free of charge via www.ccdc.cam.ac.uk/conts/retrieving.html (or from the CCDC, 12 Union Road, Cambridge CB2 1EZ, UK).
42. Supported by grants from NIH (GM-33162 and GM-38767 to L.Q. and GM-22701 to E.M.) and the Korea Science and Engineering Foundation (KOSEF) (R02-2002-000-00048-0 to W.N.), a postdoctoral fellowship from the Deutsche Forschungsgemeinschaft (J.-U.R.), and a graduate fellowship from NSF (A.S.). We also thank KOSEF and NSF for stimulating this international cooperative research effort.

Supporting Online Material

www.sciencemag.org/cgi/content/full/299/5609/1037/DC1
Materials and Methods
Fig. S1
Table S1
References

9 September 2002; accepted 10 December 2002

Crystal Structure of Naphthalene Dioxygenase: Side-on Binding of Dioxygen to Iron

Andreas Karlsson,[1] Juanito V. Parales,[2] Rebecca E. Parales,[2] David T. Gibson,[2] Hans Eklund,[1] S. Ramaswamy[3]*

Binding of oxygen to iron is exploited in several biological and chemical processes. Although computational and spectroscopic results have suggested side-on binding, only end-on binding of oxygen to iron has been observed in crystal structures. We have determined structures of naphthalene dioxygenase that show a molecular oxygen species bound to the mononuclear iron in a side-on fashion. In a complex with substrate and dioxygen, the dioxygen molecule is lined up for an attack on the double bond of the aromatic substrate. The structures reported here provide the basis for a reaction mechanism and for the high stereospecificity of the reaction catalyzed by naphthalene dioxygenase.

Oxygenases that catalyze the addition of molecular oxygen to organic substrates play a pivotal role in diverse areas such as drug metabolism and the biodegradation of environmental pollutants. Oxygen activation by cytochrome(s) P450 (*1–6*) and diiron enzymes such as methane monooxygenase (MMO) (*7–10*) have been studied in detail. In contrast, less is known about bacterial Rieske non-heme iron dioxygenases (RDOs) that catalyze the stereospecific addition of dioxygen to aromatic hydrocarbons (*11*). The reaction products are chiral arene *cis*-dihydrodiols that are of current interest in enantioselective synthesis (*12*).

Naphthalene dioxygenase (NDO) from *Pseudomonas* sp., the only RDO for which a crystal structure is known (*13*), oxidizes naphthalene to *cis*-(1*R*,2*S*)-dihydroxy-1,2-dihydronaphthalene (*14*). The enzyme has an $\alpha_3\beta_3$ composition, and each α subunit contains a Rieske [2Fe-2S] center and mononuclear iron at the active site. Electrons from the reduced form of nicotinamide adenine dinucleotide (NADH) are transferred to NDO via an iron-sulfur flavoprotein (*15*) and a Rieske ferredoxin (*16*). The subsequent steps lead to oxygen activation and the formation of naphthalene *cis*-dihydrodiol. Although several hypotheses have been advanced to account for oxygen activation and catalysis by RDOs, the reaction mechanism remains elusive (*17–21*). To understand the molecular basis for the reaction, we have formed complexes of NDO with substrates, oxygen, substrate plus oxygen, and product and have determined their structures by x-ray crystallography (Table 1).

Substrate binding was achieved by soaking crystals of NDO in ethanol solutions of the substrates as described (*22*). Indole (*22*) and naphthalene (Fig. 1A) bind in an elongated cleft, with the carbon atoms to be hydroxylated at a distance of about 4 Å from the ferrous iron at the active site (*22*). The structure, determined from crystals of NDO that were reduced with dithionite and then exposed to oxygen, reveals that dioxygen binds side-on close to the mononuclear iron at the active site (Fig. 1B). The distances between the oxygen atoms and iron are 2.2 and 2.3 Å, respectively. The distance between the oxygen atoms was originally fixed at 1.45 Å during refinement (*23*). The O-O distance, upon crystallographic refinement, converged to 1.4 Å. The refined distance between the oxygen atoms suggests that the structure contains a peroxide species, but the resolution of 1.75 Å does not definitively permit such an assignment. Nor do available spectroscopic studies give a reliable conclusion. Electron paramagnetic resonance (EPR) studies, which were done under different conditions from those of the crystallographic studies, show that a small amount of the mononuclear ferrous iron is oxidized upon exposure to oxygen when oxygen alone is allowed to react with the fully reduced enzyme (*17*). The reaction with oxygen is much faster with substrate present.

In a similar experiment, reduced crystals soaked with indole were exposed to oxygen in a pressure cell at –17°C. The structure obtained from these crystals, besides having indole bound, exhibited clear density for a dioxygen species bound side-on with both oxygens coordinated to the iron (Fig. 1C). The turnover reaction is apparently slow under these conditions because no product was visible in the electron density maps. The refined iron-oxygen distances are 1.8 and 2.0 Å and the refined distance between the oxygen atoms converges to about 1.4 Å. The temperature factors of the two oxygen atoms are higher than those of the surrounding atoms (32 and 39; Fe is 20). The bound substrate also has B-factors comparable to the dioxygen species. This indicates that the substrate and dioxygen species have high but not full occupancy. All attempts to model the structure with one bound oxygen (water/hydroxide) resulted in excess residual electron density (*23*). The structure of the fully oxidized enzyme shows that two water molecules bind differently to the ferric ion in

[1]Department of Molecular Biology, Swedish University of Agricultural Sciences, Box 590, Biomedical Center, 75124 Uppsala, Sweden. [2]Department of Microbiology and Center for Biocatalysis and Bioprocessing, [3]Department of Biochemistry, University of Iowa, Iowa City, IA 52242, USA.

*To whom correspondence should be addressed. E-mail: s-ramaswamy@uiowa.edu

a regular octahedral coordination (fig. S3), so two water molecules can be excluded as an interpretation of the ternary complex.

Both naphthalene and indole are substrates for NDO. A comparison of the binding of naphthalene and indole (*22*) in the active site of NDO shows that they bind similarly (fig. S4). It is therefore reasonable to suggest that the structure of the ternary complex of enzyme:indole:

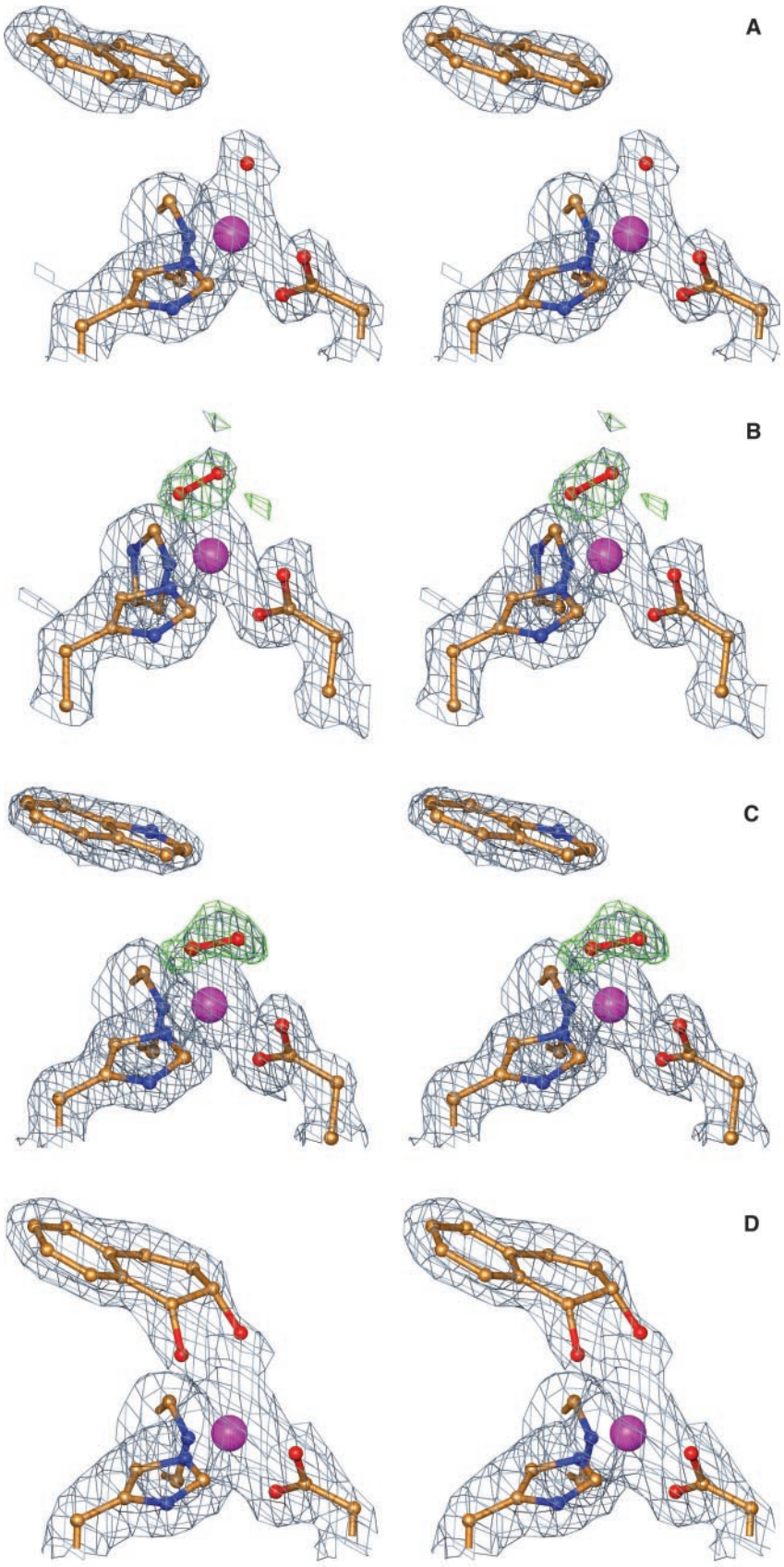

Fig. 1. (All panels are stereopairs.) (**A**) Binding of naphthalene at the active site of NDO. The gray $2F_{obs} - F_{calc}$ map is contoured at 1.0 σ. (**B**) Binding of dioxygen to the mononuclear iron in the absence of substrate. The gray $2F_{obs} - F_{calc}$ map is contoured at 1.15 σ and the green $F_{obs} - F_{calc}$ map (computed before the dioxygen molecule was modeled) at 3.8 × RMS (root mean square). (**C**) Binding of oxygen to the mononuclear iron in the presence of indole. The gray $2F_{obs} - F_{calc}$ map is contoured at 1.0 σ and the green $F_{obs} - F_{calc}$ map (computed before the dioxygen molecule was modeled) at 4.0 × RMS. (**D**) Naphthalene *cis*-dihydrodiol bound to the active site of NDO. The gray $2F_{obs} - F_{calc}$ map is contoured at 1.0 σ. Superposition of the product complex and the substrate complex shows that the positions of the rings in the product and the substrate are similar. The product cannot move any closer to the iron, as it would bring the O from the product into van der Waals short contact with the His ligand of the Fe. The current distance between the O and the N of His is 2.9 Å. Color code: yellow, carbon; blue, nitrogen; red, oxygen; purple, iron.

dioxygen also depicts the binding mode for all substrates that undergo *cis*-dihydroxylation by NDO. This ternary complex is probably as close to a reactive complex as possible, and its observation might be due to the low temperature at which the experiment was carried out.

The structure determined from NDO crystals in the resting state soaked with naphthalene *Cis*-dihydrodiol showed this product bound at the active site with both oxygen atoms coordinated to the iron (Fig. 1D). The oxygen-iron distances in this complex are longer than normal (iron-oxygen) coordination distances (2.8 Å).

In the absence of the observation of a side-on–bound dioxygen and solely on the basis of the structure of an indole-oxygen adduct, we previously suggested a sequential mechanism (*22*). The indole-oxygen adduct (*22*) left a number of questions unanswered. The structures presented here form a firm basis to propose a concerted mode of attack and provide a better explanation for the *cis*-specificity of the dihydroxylation reaction.

The series of NDO complex structures with substrate (Fig. 1A; Fig. 2A, **4**), oxygen (Fig. 1B; Fig. 2A, **3**), substrate and oxygen (Fig. 1C; Fig. 2A, **5**), and product (Fig. 1D; Fig. 2A, **6**) represent states along a reaction pathway. The arrangement of the oxygen atoms in the ternary complex (Fig. 1C; Fig. 2A, **5**) positions the oxygen atoms almost parallel to those observed in the product complex, albeit closer to the iron. Our finding that oxygen binds side-on in both a binary and a ternary complex has several important implications for the *cis*-dihydroxylation reaction catalyzed by NDO. In a side-on–bound dioxygen species, both oxygen atoms are polarized similarly. This, in addition to the geometric arrangement of the bound dioxygen species in van der Waals contact to the double bond of the substrate, suggests a concerted mechanism where both oxygen atoms react with the carbon atoms of the substrate double bond (Fig. 2B, a). Such a reaction would explain the characteristic *cis*-stereospecific addition of both oxygen atoms to substrates by NDO.

Further investigation will be needed to determine whether the reactive peroxide is protonated (Fig. 2B, b). If protonated, protons are probably delivered through a water channel connected to Asn^{201}, which is at hydrogen bond distance to the bound dioxygen species. This intermediate could be formed in the reaction of

Table 1. Data collection and refinement details of the four structures reported. Numbers in parentheses indicate the last resolution shell. All crystallographic refinement was carried out with the program Refmac5.

	Structure (enzyme +) complex			
	Naphthalene	Dioxygen	Dioxygen + indole	Product
Space group	*R*32	*R*32	*R*32	*R*32
Cell dimensions $a = b$, c (Å)	139.7, 208.1	140.3, 208.8	139.8, 208.9	139.7, 208.4
Resolution range (Å)	20 to 1.7	30 to 1.75	40 to 1.4	30 to 1.95
Completeness (%)	95.9 (97.5)	94.0 (86.5)	96.0 (88.9)	99.8 (100.0)
R_{sym} (%)	5.7 (19.3)	6.3 (32.1)	6.2 (35.7)	7.0 (25.4)
$I/\sigma I < 2$ (%)* or $(I/\sigma I)$†	8.4 (24.4)	10.2 (2.2)	6.3 (2.1)	11.3 (32.1)
Number of observations	450,209	293,928	648,676	493,885
Unique reflections	82,025	80,092	147,355	56,759
Wavelength (Å)	0.9315	1.54	0.934	0.931
Beamline	ID14-4	Rotating anode	ID14-1	ID14-4
Temperature (K)	100	100	100	100
R factor (%)	16.3	17.8	18.9	18.3
R_{free} (%)	18.7	18.8	20.0	21.7
RMSD bond lengths (Å)	0.019	0.014	0.016	0.018
RMSD bond angles (°)	1.811	1.629	1.697	1.799
Evaluation program	DENZO	d*trek	MOSFLM	DENZO
Scaling program	SCALEPACK	d*trek	SCALA	SCALEPACK
Refinement program	Refmac5	Refmac5	Refmac5	CNS/Refmac5

*Percentage of data with $I/\sigma I < 2$, represented for data scaled with SCALEPACK (*30*). †$I/\sigma I$ represented for data scaled with SCALA (CCP4) or d*trek (*31*).

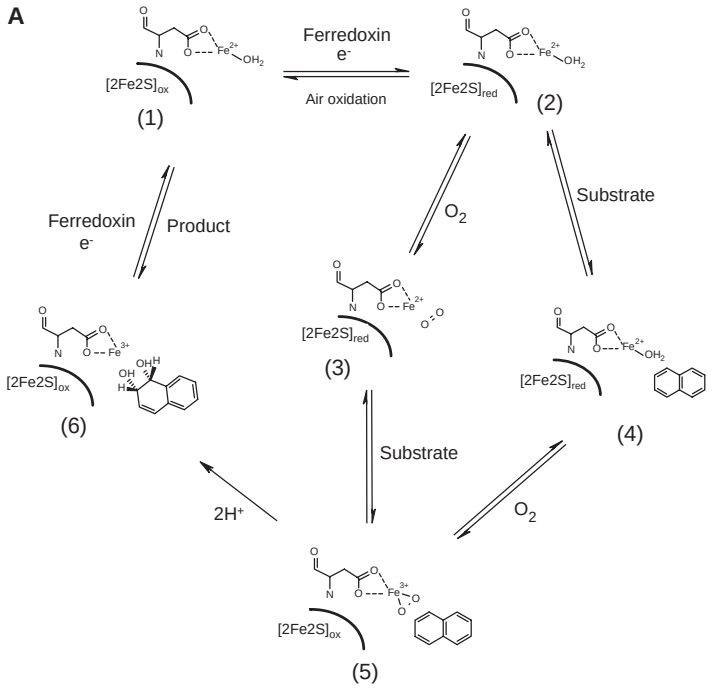

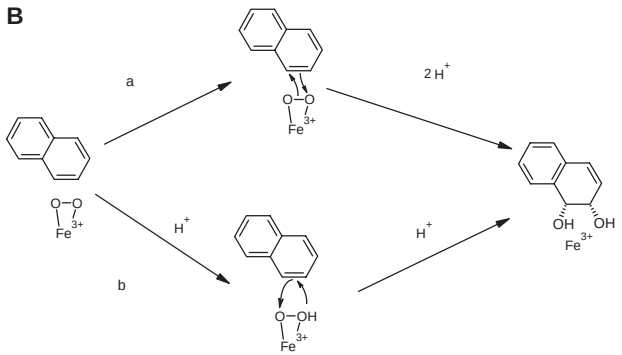

Fig. 2. (**A**) Scheme showing how the different structures in Fig. 1 can be arranged to follow the dihydroxylation reaction catalyzed by NDO. Naphthalene and indole are both substrates for the enzyme, and we have used them interchangeably in different studies of the enzyme (*23*). For simplicity we show only naphthalene here. The structures are as follows: **1**, the resting enzyme with oxidized Rieske center and ferrous active site [Protein Data Bank (PDB) code 1O7H]; **2**, the reduced enzyme (PDB code 1O7W); **3**, binary dioxgen complex (PDB code 1O7M); **4**, binary substrate complex, structures with both indole and naphthalene [PDB codes 1EG9 (indole) and 1O7G (naphthalene)]; **5**, ternary substrate dioxygen species, structure with indole (PDB code 1O7N); and **6**, product naphthalene *cis*-1,2-dihydrodiol (PDB code 1O7P). [2Fe-2S] refers to the nearest Rieske iron-sulfur cluster. (**B**) Chemical steps in the dioxygenation reaction carried out by Rieske dioxygenases.

NDO with oxygen or hydrogen peroxide, as proposed by Wolfe and Lipscomb (*17, 18*).

The unique feature of NDO that sets it apart from P450 is its ability to catalyze stereospecific addition of dioxygen to aromatic compounds, resulting in the formation of *cis*-dihydrodiols (*12, 24*). For cytochrome P450 and MMO, transient high iron oxidation states are required for the necessary oxygen cleavage (*25*); this is not the case for NDO, where both atoms of dioxygen react in concert with the substrate. The four electrons required for catalysis are one each from the active-site ferrous iron and the Rieske center, and two from the double bond of the substrate. An important difference in the geometry of the active sites of cytochrome P450 and NDO is that the active-site iron is highly accessible in NDO, with a large part of its surface available for the binding of both oxygen atoms to iron. The favorable position of the substrate and Asn^{201} further favors side-on binding. It is possible that for cytochrome P450 and other heme proteins, the presence of the planar heme group reduces the accessible surface of iron, resulting in an end-on binding of oxygen.

We have directly observed a side-on dioxygen species bound to iron. Computational studies (*26*) have predicted the existence of this species, and there are spectroscopic data consistent with side-on binding (*27, 28*). We suggest that side-on binding of oxygen as a starting point for oxygen activation by NDO has direct implications for the mechanism of dihydroxylation of NDO in terms of the stereo- and regiospecific reactions catalyzed by the enzyme (*29*). The results presented here provide a new basis for further computational and structural investigations of oxygen activation by biological systems and may facilitate the design of chemical catalysts capable of *cis*-dihydroxylation.

References and Notes

1. I. Schlichting *et al*., *Science* **287**, 1615 (2000).
2. T. L. Poulos, *Curr. Opin. Struct. Biol.* **5**, 767 (1995).
3. _____, B. C. Finzel, I. C. Gunsalus, G. C. Wagner, J. Kraut, *J. Biol. Chem.* **260**, 6122 (1985).
4. T. L. Poulos, B. C. Finzel, A. J. Howard, *Biochemistry* **25**, 5314 (1986).
5. T. L. Poulos, R. Raag, *FASEB J.* **6**, 674 (1992).
6. H. Y. Li, S. Narasimhulu, L. M. Havran, J. D. Winkler, T. L. Poulos, *J. Am. Chem. Soc.* **117**, 6297 (1995).
7. B. J. Wallar, J. D. Lipscomb, *Chem. Rev.* **96**, 2625 (1996).
8. A. C. Rosenzweig, C. A. Frederick, S. J. Lippard, P. Nordlund, *Nature* **366**, 537 (1993).
9. A. C. Rosenzweig, P. Nordlund, P. M. Takahara, C. A. Frederick, S. J. Lippard, *Chem. Biol.* **2**, 409 (1995).
10. J. D. Lipscomb, *Annu. Rev. Microbiol.* **48**, 371 (1994).
11. D. T. Gibson, R. E. Parales, *Curr. Opin. Biotechnol.* **11**, 236 (2000).
12. T. Hudlicky, D. Gonzalez, D. T. Gibson, *Aldrichim. Acta* **32**, 35 (1999).
13. B. Kauppi *et al*., *Structure* **6**, 571 (1998).
14. A. M. Jeffrey *et al*., *Biochemistry* **14**, 575 (1975).
15. B. E. Haigler, D. T. Gibson, *J. Bacteriol.* **172**, 457 (1990).
16. _____, *J. Bacteriol.* **172**, 465 (1990).
17. M. D. Wolfe, J. V. Parales, D. T. Gibson, J. D. Lipscomb, *J. Biol. Chem.* **276**, 1945 (2001).
18. M. D. Wolfe, J. D. Lipscomb, *J. Biol. Chem.* **278**, 829 (2003).
19. M. D. Wolfe *et al*., *Biochemistry* **41**, 9611 (2002).
20. K. Chen, L. Que, *Angew. Chem. Int. Ed.* **38**, 2227 (1999).
21. K. Chen, M. Costas, J. Kim, A. K. Tipton, L. Que Jr., *J. Am. Chem. Soc.* **124**, 3026 (2002).
22. E. Carredano *et al*., *J. Mol. Biol.* **296**, 701 (2000).
23. See supporting data on *Science* Online.
24. D. R. Boyd, G. N. Sheldrake, *Nat. Prod. Rep.* **15**, 309 (1998).
25. D. L. Harris, *Curr. Opin. Chem. Biol.* **5**, 724 (2001).
26. S. Ahmad *et al*., *Inorg. Chem.* **27**, 2230 (1988).
27. F. Neese, E. I. Solomon, *J. Am. Chem. Soc.* **120**, 12829 (1998).
28. F. Mather *et al*., *J. Am. Chem. Soc.* **124**, 4966 (2002).
29. S. M. Resnick, K. Lee, D. T. Gibson, *J. Ind. Microbiol.* **17**, 438 (1996).
30. Z. Otwinowski, *Data Collection and Processing* (Daresburry Laboratories, Warrington, UK, 1993), pp. 56–62.
31. J. W. Pflugrath, *Acta Crystallogr.* **D55**, 1718 (1999).

32. We thank J. Hajdu and his group at Uppsala for help in carrying out several experiments; M. Niebergall for helpful tips; several synchrotron stations and beam lines for help with data collection (European Synchrotron Radiation Facility, Grenoble, Max Lab, Lund, and Industrial Macromolecular Crystallography Association–Collaborative Access Team, Advanced Photon Source); and J. Lipscomb for helpful discussions. Supported by the Swedish Research Council for Environment, Agricultural Science, and Spatial Planning (H.E. and S.R.), the Swedish Research Council (H.E.), and U.S. Public Health Service grants GM62904 (S.R.) and GM29909 (D.T.G.).

Supporting Online Material

www.sciencemag.org/cgi/content/full/299/5609/1039/DC1
Materials and Methods
References
Figs. S1 to S4

3 September 2002; accepted 19 December 2002

Carbon Nanotube Flow Sensors

Shankar Ghosh,[1] A. K. Sood,[1]* N. Kumar[2]

We report that the flow of a liquid on single-walled carbon nanotube bundles induces a voltage in the sample along the direction of the flow. The voltage that was produced fit a logarithmic velocity dependence over nearly six decades of velocity. The magnitude of the voltage depended sensitively on the ionic conductivity and on the polar nature of the liquid. Our measurements suggest that the dominant mechanism responsible for this highly nonlinear response involves a direct forcing of the free charge carriers in the nanotubes by the fluctuating Coulombic field of the liquid flowing past the nanotubes. We propose an explanation based on pulsating asymmetric ratchets. Our work highlights the device potential for nanotubes as sensitive flow sensors and for energy conversion.

Carbon nanotubes are currently being studied in an effort to understand their novel structural, electronic, and mechanical properties and to explore their immense potential for many applications in nanoelectronics (*1*), and as actuators (*2*) and sensors (*3*). A metallic single-walled carbon nanotube (SWNT), which is a low-dimensional system, has electrons that form a strongly correlated liquid, called a Luttinger liquid (*4*). This liquid shows a separation of spin and charge and demonstrates the associated characteristic power-law dependence of the nanotube resistance on the bias voltage and temperature. Král and Shapiro (*5*) also showed theoretically the generation of an electric current in a metallic carbon nanotube immersed in a flowing liquid. One mechanism they proposed for the generation of the electric current and voltage is the transfer of momentum from the flowing liquid molecules to the acoustic phonons in the nanotube as the phonon quasi-momentum, which in turn drags free charge carriers in the nanotube. Another mechanism noted by these authors involves a direct scattering of the free carriers from the fluctuating Coulombic fields of the ions or polar molecules in the flowing liquid. They argued, however, that the latter mechanism creates a current that is five orders of magnitude smaller than the current that results from the phonon-induced electron drag.

We report the experimental observation of the voltage generated by the flow of a polar liquid over SWNT bundles. It was observed that the induced voltage tends to saturate at flow velocities as low as 10^{-5} m/s. The observed data can be fitted empirically to a logarithmic dependence of the voltage on the flow velocity, in sharp contrast to the linear dependence predicted by Král and Shapiro (*5*). The magnitude of the voltage induced along the nanotube by the flow depends significantly on the ionic strength of the flowing liquid, suggesting that the mechanism involving fluctuating Coulombic fields dominates that of the phonon-mediated electron drag. This has led us to propose a mechanism for the observed flow-induced voltage based on a pulsating asymmetrical thermal ratchet model. This mechanism involves the fluctuating Coulombic potentials that result from the ionic liquid in flow, where the asymmetry is provided by the velocity gradient (shear) at the liquid-solid interface.

[1]Department of Physics, Indian Institute of Science, Bangalore 560 012, India. [2]Raman Research Institute, C.V. Raman Avenue, Bangalore 560 080, India.

*To whom correspondence should be addressed. E-mail: asood@physics.iisc.ernet.in